

Galaxy Clustering Evolution in the CNOC2 High-Luminosity Sample

R. G. Carlberg^{1,2}, H. K. C. Yee^{1,2}, S. L. Morris^{1,3}, H. Lin^{1,2,4,5},
P. B. Hall^{1,2}, D. Patton^{1,6}, M. Sawicki^{1,2,7}, and C. W. Shepherd^{1,2}

Received _____; accepted _____

¹Visiting Astronomer, Canada–France–Hawaii Telescope, which is operated by the National Research Council of Canada, le Centre National de Recherche Scientifique, and the University of Hawaii.

²Department of Astronomy, University of Toronto, Toronto ON, M5S 3H8 Canada

³Dominion Astrophysical Observatory, Herzberg Institute of Astrophysics, , National Research Council of Canada, 5071 West Saanich Road, Victoria, BC, V8X 4M6, Canada

⁴Steward Observatory, University of Arizona, Tucson, AZ, 85721

⁵Hubble Fellow

⁶Department of Physics & Astronomy, University of Victoria, Victoria, BC, V8W 3P6, Canada

⁷Mail Code 320-47, Caltech, Pasadena 91125, USA

ABSTRACT

The redshift evolution of the galaxy two-point correlation function is a fundamental cosmological statistic. To identify similar galaxy populations at different redshifts, we select a strict volume-limited sample culled from the 6100 cataloged CNOC2 galaxies. Our high-luminosity subsample selects galaxies having k -corrected and evolution-compensated R luminosities, $M_R^{k,e}$, above -20 mag ($H_0 = 100 \text{ km s}^{-1} \text{ Mpc}^{-1}$) where $M_*^{k,e}(R) \simeq -20.3$ mag. This subsample contains about 2300 galaxies distributed between redshifts 0.1 and 0.65 spread over a total of 1.55 square degrees of sky. A similarly defined low-redshift sample is drawn from the Las Campanas Redshift Survey. We find that the co-moving two-point correlation function can be described as $\xi(r|z) = (r_{00}/r)^\gamma (1+z)^{-(3+\epsilon-\gamma)}$ with $r_{00} = 5.03 \pm 0.08 h^{-1} \text{ Mpc}$, $\epsilon = -0.17 \pm 0.18$ and $\gamma = 1.87 \pm 0.07$ over the $z = 0.03$ to 0.65 redshift range, for $\Omega_M = 0.2, \Lambda = 0$. The measured clustering amplitude and its evolution are dependent on the adopted cosmology. The measured evolution rates for $\Omega_M = 1$ and flat $\Omega_M = 0.2$ background cosmologies are $\epsilon = 0.80 \pm 0.22$ and $\epsilon = -0.81 \pm 0.19$, respectively, with r_{00} of $5.30 \pm 0.1 h^{-1} \text{ Mpc}$ and $4.85 \pm 0.1 h^{-1} \text{ Mpc}$, respectively. The sensitivity of the derived correlations to the evolution corrections and details of the measurements is presented. The analytic prediction of biased clustering evolution for only the low density, Λ CDM cosmology is readily consistent with the observations, with biased clustering in an open cosmology somewhat marginally excluded and a biased $\Omega_M = 1$ model predicting clustering evolution that is more than 6 standard deviations from the measured value.

Subject headings: cosmology: large scale structure, galaxies: evolution

1. Introduction

The measurement of the evolution of galaxy clustering is a direct test of theories of the evolution of structure and galaxy formation in the universe. Clustering is predicted to change with increasing redshift in a manner that depends on the background cosmology, the spectrum of primordial density fluctuations out of which clustering grows, and the relation of galaxies to dark matter halos. Specific predictions of clustering growth are available for a range of CDM-style cosmological models and galaxy identification algorithms. As a result of biasing (Kaiser 1984) there is a physically important generic prediction that the clustering of normal galaxies should not be identical to dark matter clustering and their clustering should evolve slowly at low redshifts. More generally, clustering evolution is of interest for its impact on galaxies, since clustering leads to galaxy-galaxy merging and creates the groups and clusters in which galaxies are subject to high gas densities and temperatures not found in the general field.

The theoretical groundwork to interpret the quantitative evolution of dark matter clustering and the trends of galaxy clustering evolution is largely in place for hierarchical structure models. Although the details of the mass buildup of galaxies and the evolution of their emitted light are far from certain at this time, clustering of galaxies depends primarily on the distribution of initial density fluctuations on the mass scale of galaxies. N-body simulations of ever growing precision along with their theoretical analysis (*e.g.*, Davis et al. 1985; Pearce et al. 1999) have led to a good semi-analytic understanding of dark matter clustering into the nonlinear regime. One result is a remarkable, convenient, theoretically motivated, empirical equation that relates the linear power spectrum and its nonlinear outcome (Efstathiou Davis White & Frenk 1985; Hamilton et al. 1991; Peacock & Dodds 1996). This allows an analytic prediction of the clustering evolution of the dark matter density field.

Normal galaxies, which are known to exist near the centers of dark matter halos with velocity dispersions in the approximate range of 50 to 250 km s^{-1} , cannot have a clustering evolution identical to the full dark matter density field. Kaiser (1984) showed that the dense “peaks” in the initial density field that ultimately collapse to form halos are usually more correlated than the full density field. For high peaks, the peak-peak correlation, $\xi_{\nu\nu}(r|z)$, is approximately $[\nu/\sigma(z)]^2$ times the correlation of the full dark matter density field, $\xi_{\rho\rho}(r|z)$, (see Mo & White 1996 for a more general expression) where ν measures the minimal “peak height” for formation of a halo, in units of the variance on that mass scale, $\sigma(M, z)$ (Bardeen et al. 1986). Both $\sigma^2(M, z)$ and $\xi_{\rho\rho}(z, r)$ (in co-moving co-ordinates) grow approximately as $D^2(z, \Omega)$ (exactly so in the linear regime), where $D(z, \Omega)$ is the growth factor for density perturbations in the cosmology of interest. The result is that $\xi_{\nu\nu}(r|z)$ stays nearly constant in co-moving co-ordinates. This result is approximately verified in n-body experiments (Carlberg & Couchman 1989; Carlberg 1991; Colin Carlberg & Couchman 1997; Jenkins et al. 1998) which can be accurately modeled with a theoretically motivated analytic function (Mo & White 1996). An implication is that dark matter halo clustering evolution will have little sensitivity to the background cosmology (Governato et al. 1998; Pearce et al. 1999). These results formally apply to low density “just virialized” halos, whereas galaxies are found in the dense central regions of dark matter halos. Therefore the clustering of galaxies needs to take into account their dissipation relative to the (presumed) dissipationless dark matter. Dissipationless n-body simulations which resolve sub-halos within larger virialized units provide the basic dynamical information but still require a theory of galaxy formation to associate them with luminous objects, as guided by observations such as we report here.

At low redshift there have been several substantial clustering surveys, deriving information from both angular correlations, which can be de-projected with non-evolving luminosity functions, and redshift surveys, where the kinematics of the galaxies provides

additional information about clustering dynamics. The observational measurement of clustering at higher redshifts has yet to reach the size, scale coverage, or redshift precision of the pioneering low redshift CfA survey (Davis & Peebles 1983). Angular correlations of galaxies at higher redshifts provide some insights, but inevitably mix different galaxy populations at different redshifts and require an accurate $n(z)$ to break the degeneracy between an evolving luminosity function and an evolving clustering amplitude (Infante & Pritchett 1995; Postman et al. 1998; Connolly Szalay & Brunner 1998). There are two redshift surveys extending out to $z \simeq 1$, the Canada France Redshift Survey (Lilly et al. 1995) and the Hawaii K survey (Cowie et al. 1996). Measurement of the correlation evolution of the galaxies in these surveys found a fairly rapid decline in clustering with redshift (LeFèvre et al. 1996; Carlberg et al. 1997). Neither analysis took into account the evolution of the luminosity function or was able to quantify the effects of the small sky areas containing the samples. Recently two relatively large sky area samples, a preliminary analysis of the survey reported in this paper (Carlberg et al. 1998) and a shallower limiting magnitude survey (Small et al. 1998), have indicated much stronger correlations at about redshift $z \simeq 0.3$ than the earlier small area surveys.

This is the first in a series of papers which discusses the clustering and kinematic properties of the Canadian Network for Observational Cosmology field galaxy redshift survey. (Yee et al. 2000). The CNOC2 survey is designed to be comparable in size and precision to the first CfA redshift survey (Davis & Peebles 1983) but covering galaxies out to redshift 0.7. In this paper we restrict our analysis to measurements of the correlation amplitude of the high-luminosity galaxies in the CNOC2 redshift survey, which are a particularly simple and interesting subsample. The CNOC2 luminosity function is known in considerable detail (Lin et al. 1999) which allows us to define an evolution-compensated volume limited sample thereby creating a straightforward sample to analyze.

The next section of the paper briefly discusses the CNOC2 sample and the volume limited subsample of high-luminosity galaxies. Section 3 describes in detail our estimate of the projected correlation function and its errors, along with its sensitivity to various possible systematic errors. Section 4 reports our best estimates of the evolution of high-luminosity galaxy clustering in a variety of cosmologies. The results are discussed and conclusions drawn in Section 5. Throughout this paper we use $H_0 = 100h \text{ km s}^{-1} \text{ Mpc}^{-1}$ as various cosmologies as specified.

2. The CNOC2 Sample

The Canadian Network for Observational Cosmology (CNOC) field galaxy redshift survey is designed to investigate nonlinear clustering dynamics and its relation to galaxy evolution on scales smaller than approximately $20h^{-1} \text{ Mpc}$ over the $0 \leq z \leq 0.7$ range. There is substantial galaxy evolution over this redshift range (Broadhurst Ellis & Shanks 1988; Ellis et al. 1996; Lilly et al. 1995; Cowie et al. 1996; Lin et al. 1999) for which the physical cause is unclear. The issues in designing a dynamically useful redshift survey are centered around efficiently and economically obtaining sufficient data to conclusively answer the questions posed about the evolution of clustering in galaxies and the dark matter. At these relatively modest redshifts the galaxies have spectra whose lines are within the range where efficient multi-object spectrographs allow velocities with a precision comparable to local surveys can be obtained. The observational procedures build on those for the CNOC1 cluster redshift survey (Yee Ellingson & Carlberg 1996), although there are considerable differences of detail. The strategy and procedures are discussed in greater detail in the CNOC2 methods paper (Yee et al. 2000).

A representative volume in the universe must contain a reasonable number of low richness clusters and a good sampling of $50 h^{-1} \text{ Mpc}$ voids, or equivalently the “cosmic”

variance from one sample to another of equivalent design, but different sky positions, should not be too large. Taking a CDM spectrum (with $\sigma_8 = 1$ and $\Gamma_s = 0.2$; see Efstathiou, Bond & White 1992) as a guide we find that even a $50h^{-1}$ Mpc sphere, with enclosed volume of about $0.5 \times 10^6 h^{-3} \text{Mpc}^3$, has an expected dispersion in galaxy numbers of approximately 17%. However, a spherical geometry is an ideal not available to relatively narrow angle surveys. The best available option is to spread the area of the survey over several independent patches on the sky. Each patch should subtend an angle exceeding the correlation length. At $z = 0.4$ a patch 0.5 degree across subtends $8.8 h^{-1}$ Mpc (co-moving, for $\Omega_M = 0.2, \Omega_\Lambda = 0$) which turns out to be about two correlation lengths. We can crudely approximate the survey as a set of cylinders or spheres arranged in a row. A sphere of radius the correlation length (whatever that happens to be) has an expected variance of about $3/(3 - \gamma)$ in the numbers of galaxies (Peebles 1980), where $\gamma = 1.8$ is the approximate slope of the power law portion of the correlation function. Over our redshift range there will be about 200 of these spheres in our sample, which if we divide into bins of 50, statistically reduces the variance in binned counts to about 30%. The observational practicalities of always having a field accessible at modest airmass, control over patch to patch variations, and the constraint of not unduly fragmenting the survey area, indicate that we need a minimum of four and no more than about eight of these patches. We choose four. The resulting survey is well suited to measuring the evolution of correlations.

The CNOC2 survey is contained in four patches on the sky. Each patch consists of a central block, roughly 30 arcminutes on a side, with two “legs”, 10 arcminutes wide and about 40 arcminutes in extent, to provide an estimate of the effects of structure on larger scales. The resulting total sky area is about 1.55 square degrees. The sampled volume is about $0.5 \times 10^6 h^{-3} \text{Mpc}^3$, roughly comparable to the low redshift CfA survey used for similar measurements at low redshift (Davis & Peebles 1983) which had 1230 galaxies in the “semi-volume limited” Northern sample from which the correlation length was derived.

The redshift range targeted, 0.1 to about 0.7, suggests we set the limiting magnitude at $R = 21.5$ magnitude, which gives a median redshift of about 0.4. At this limit the sky density is about 6000 galaxies per square degree yielding a photometric sample of about 10,000 galaxies to the spectroscopic limit.

Photometry is obtained in the UBVRI bands, with the R-band fixing the sample limit at 21.5 mag. The R filter has the important feature of always being redward of the 4000Å break over our redshift range. The other bands provide information useful for determining appropriate k-corrections and separating galaxies into types of different evolutionary state (an issue not considered in this paper). The spectra are band-limited with a filter that restricts the range to 4390-6293Å. The S/N and spectral resolution give an observed frame velocity error of about 100 km s^{-1} , as determined by comparison of independent spectra of the same objects. In total there are about 6000 galaxies with redshifts in our sample.

At low redshift we will use the Las Campanas Redshift Survey (LCRS) to provide a directly comparable sample. The LCRS is an R-band selected survey (Shectman et al. 1996) that covers the redshift range 0.033 to 0.15, with R magnitudes restricted to 15.0 and 17.7 mag. The bright magnitude limit leads to higher luminosity galaxies being depleted at low redshifts. The LCRS's selection function varies from field to field and under samples galaxies with separations less than about $100 h^{-1} \text{ kpc}$. We compute both magnitude and geometric weights using the approach adopted in the CNOC cluster redshift survey (Yee Ellingson & Carlberg 1996) but smoothing over a circle of 0.4 degree. The same procedures are used for the CNOC2 data, using a smoothing radius of 2 arcminutes. The same correlation analysis programs were used for the LCRS and CNOC2 data. The only differences are that the LCRS data are not k-corrected and are analyzed for a single cosmological model, $\Omega_M = 0.2, \Omega_\Lambda = 0$.

2.1. The High-Luminosity Subsample

In order to determine how clustering evolves we must measure the correlations of a statistically identical population of galaxies at increasing redshifts, which demands a secure statistical knowledge of the evolution of the galaxy luminosity function. Individual galaxy luminosities change through stellar evolution, new star formation and merging with other galaxies. All of this would have no effect if galaxy correlations were independent of their mass and luminosity. However, there is a strong theoretical expectation that galaxy clustering will increase with mass and hence luminosity (Kaiser 1984) and there is growing evidence that the effect is observationally present at both low (Loveday et al. 1995) and intermediate redshifts (Carlberg et al. 1998). The practical issue is to define samples at different redshifts which can be sensibly compared. If the evolution is purely in luminosity, then we would want to compensate for the luminosity evolution so that the sample limit brings in galaxies of the same intrinsic luminosity at all redshifts. This would identify the same galaxies at all times. If evolution was pure merging, with no star formation, then it is particular interest to compare the clustering of galaxies of the same total stellar mass at different redshifts. As a currently practical stand-in for stellar mass we use the k-corrected and evolution compensated R-band absolute luminosity.

Our study of the CNOC2 luminosity function evolution (Lin et al. 1999) found that the R-band evolution of the k-corrected galaxy luminosity function could be approximated as pure luminosity evolution at a rate,

$$M_R^k(z) = M_R^{k,e} - Qz, \quad (1)$$

with a mean $Q \simeq 1$ (Lin et al. 1999). Equation 1 defines the k-corrected and evolution-compensated R absolute magnitudes that we use to select the sample for analysis.

Figure 1 plots $M_R^{k,e}$ as a function of redshift for the entire flux limited, $m_R \leq 21.5$ mag, CNOC2 sample. It is not necessary to know the fractional completeness for a correlation

measurement. Our correlation analysis will use galaxies with $M_R^{k,e} \leq -20$ mag, which defines a volume limited sample over the $0.1 \leq z \leq 0.65$ range. Our resulting subsample (for $\Omega_M = 0.2, \Omega_\Lambda = 0$) contains 2285 galaxies. The alternate cosmological models considered below lead to slightly different absolute magnitudes and sample sizes.

Beyond $z \simeq 0.55$ the limited CNOC2 spectral band pass leads to a lower probability that a redshift will be obtained for redder galaxies (Lin et al. 1999; Yee et al. 2000). This may lead to an erroneously low correlation in this redshift range. However, as far as we can tell from the correlation statistics, the high-luminosity galaxies for which we do have redshifts in this range have correlations statistically consistent with a smooth continuation of those at lower redshift.

The LCRS data are evolution-compensated with the same Q as the CNOC2 data, although at a mean redshift of about 0.1, this makes very little difference. The resulting low-redshift subsample derived from LCRS contains 12467 galaxies for the correlation analysis.

3. Real Space Correlations

The goal of this paper is to estimate the evolution of the clustering of a well defined population of galaxies. The CNOC2 sample is designed to measure nonlinear clustering on scales of $10h^{-1}$ Mpc and less, where clustering is quite naturally measured in terms of the two-point correlation function, $\xi(r)$. This function measures the galaxy density excess above the mean background density, n_0 , at distance r from a galaxy, $n(r) = n_0[1 + \xi(r)]$ (Peebles 1980). Measurement of the real space correlation function $\xi(r)$ is not straightforward with redshift space data. The projected real space correlation function, w_p , removes the peculiar velocities of redshift space at the cost of making a choice

for the length of the redshift column over which the integration is done. The correlation function is a measure of the variation in galaxy numbers from one volume to another. The measurement technique can easily and fairly subtly either artificially increase or decrease the variation around the estimated mean. Our survey was designed to have enough redundancy to explicitly test for a number of these effects.

We will represent the evolving correlations with a double power law model. That is, over the range of scales that we are investigating the two point correlation is well represented as a power law $\xi(r|z) = [r_0(z)/r]^\gamma$. Furthermore, the evolution of ξ is accurately described, over the redshift range we investigate, with the “ ϵ ” model, $\xi(r|z) = \xi(r|0)(1+z)^{-(3+\epsilon)}$, if lengths are measured in physical co-ordinates (Groth & Peebles 1977; Koo & Szalay 1984). In this equation the factor of $(1+z)^{-3}$ allows for the change in the mean density of galaxies due to expansion. Consequently, if the universe consists of a set of physically invariant clusters in a smooth background, then $\epsilon = 0$. A clustering pattern that is fixed in co-moving co-ordinates would have $\epsilon = \gamma - 3$, approximately -1.2 for our mean γ . A positive ϵ indicates a decline of the physical clustered density with increasing redshift, as might be expected if clustering is growing. Combining these two power law equations gives the double power law ϵ model, $\xi(r|z) = (r_{00}/r)^\gamma(1+z)^{-(3+\epsilon)}$, in physical co-ordinates, or, rewritten in co-moving co-ordinates,

$$r_0(z) = r_{00}(1+z)^{-(3+\epsilon-\gamma)/\gamma}. \quad (2)$$

The following sections discuss the steps leading up to our measurement and modeling of the co-moving $r_0(z)$. First we measure the unclustered distribution $n(z)$, then the projected real space correlation function $w_p(r_p)$ (after choosing the appropriate redshift space integration limit R_p), fit those values to the projection of $\xi(r) = (r_0/r)^\gamma$, estimate random errors, do a χ^2 fit to determine the evolution parameter ϵ and finally discuss the systematic errors.

3.1. The Unclustered Distribution

A crucial operational detail of correlation measurements is to accurately assess the mean unclustered density as a function of redshift. Once the smooth $n(z)$ is known, then we follow the usual procedure and generate a random sample which follows the redshift distribution of the data as if they were unclustered. We generate uniform random positions in the sky area occupied by the galaxies, as approximated by a series of rectangles. Correlations are then readily measured as the ratio of the number of galaxy-galaxy pairs to galaxy-random pairs. The use of a sample uniformly distributed on the sky assumes that there are no angular selection effects. For instance, crowding of spectrographic fibres causes the LCRS to be strongly under-sampled for pairs closer than $100h^{-1}$ kpc. The CNOC2 spectroscopic sample was double masked to try to fairly sample all pair separations. Slit crowding still leads to some under sampling in CNOC2 (Yee et al. 2000). Consequently we leave these small scales out of all our fits. To minimize other geometric effects, we apply to both samples an explicit geometric weight, calculated following the procedures of Yee, Ellingson & Carlberg (1996). Comparison with unweighted correlations shows that this makes little practical difference to the resulting CNOC2 correlations, since the corrections are 10% or so in the mean.

One approach to generating an unclustered distribution in redshift is to use the luminosity function, which can be estimated using maximum-likelihood techniques that are insensitive to the clustering. The complication here is that the luminosity functions need to be generated taking into account the magnitude selection function, in which only about half of the galaxies within the photometric limit have redshifts. Moreover, the selection function is magnitude dependent. A more direct approach is to model directly the redshift distribution of the selected subsample. We chose a model function having sufficiently few parameters that it is not very sensitive to the details of the clustering that are present. As

our fitting function we adopt a Maxwellian form,

$$n(z|\sigma_z, z_p) = n_0 z^2 \exp \left[-\frac{1}{2} \left(\frac{z - z_p}{\sigma_z} \right)^2 \right], \quad (3)$$

where σ_z and z_p are fitting parameters. This function was arrived at after trying various combinations of exponential cutoffs and power law rises at low redshifts, including log-normal types of distributions. The resulting form is both simple and adequately describes the data. We use a maximum likelihood approach to find the parameters of this function. The logarithm of the likelihood is $\log(L) = \sum \log(L_i)$, where the individual likelihoods are,

$$L_i(z|\sigma_z, z_p) = \frac{n(z|\sigma_z, z_p)}{\int_{z_b}^{z_t} n(z|\sigma_z, z_p) dz}. \quad (4)$$

The redshift range z_b to z_t for the fit is taken as 0.05 to 0.70 for the CNOC2 sample, although we only use the data between redshift 0.10 and 0.65. The redshift limits are 0.033 and 0.15 for the LCRS. The CNOC2 redshift distribution in bins of $\Delta z = 0.01$ for all four patches and the resulting fit is shown in Figure 2 in bins of $\Delta z = 0.01$. The best overall fit has $\sigma_z \simeq 0.18$ and $z_p \simeq 0.230$. If the strong clustering feature at $z \simeq 0.15$ in the 2148-05 patch is not included, then the fits to the individual fields are all consistent with the global fit.

Inserted into the Figure 2 is a panel showing the 68, 90 and 99% confidence contours from the maximum likelihood fit. The error is about 10% in the z_p parameter and 5% in σ_z . Given these well defined parameters we find that the 68% confidence $n(z)$ range is about 10% at any redshift we use in the analysis. This is sufficient to measure correlations to 20% precision with respect to the background out to about 2 correlation lengths. A small systematic effect visible in a $\Delta z = 0.001$ version of the $n(z)$ plot is that there are small redshift “notches” at 0.496 and 0.581 when the [OII] line falls on the 5577Å or 5892Å night sky line, respectively. This leads to an underestimate of the true mean density in the 0.45-0.55 and 0.55-0.65 redshift bins. This will bias the derived r_0 upwards in these two

redshift bins about 2% and 5% respectively, which is within our random errors.

3.2. The Projected Real Space Correlation Function

The correlation function is a real space quantity, whereas the redshift space separation of two galaxies depends on their peculiar velocities as well as the physical separation. Although the peculiar velocities contain much useful information about clustering dynamics, they are an unwanted complication for the study of configuration space correlations. The peculiar velocities are eliminated by integrating over the redshift direction to give the projected correlation function,

$$w_p(r_p) = \int_{-R_p}^{R_p} \xi(\sqrt{r_p^2 + r_z^2}) dr_z \quad (5)$$

(Davis & Peebles 1983). If we take a power law correlation $\xi(r) = (r_0/r)^\gamma$ and integrate to $R_p = \infty$ we find, $w_p(r_p)/r_p = \Gamma(1/2)\Gamma((\gamma - 1)/2)/\Gamma(\gamma/2)(r_0/r_p)^\gamma$ (Peebles 1980). However, in a practical survey, summing over ever increasing distances leads to little increase in the signal and growing noise from fluctuations in the field density. The signal-to-noise considerations in the choice of R_p are straightforward. To capture the bulk of the correlation signal, R_p should be significantly larger than the local r_0 and the length corresponding to the pairwise velocity dispersion, $\sigma_{12}/H(z)$. These are both about 3 or 4 h^{-1} Mpc. Large values, say $R_p \simeq 100h^{-1}$ Mpc, might more completely integrate the correlation signal but they do so at the considerable cost of increased noise. Exactly where to terminate the integration depends greatly on the range of correlations of interest. Here we are focussed on the non-linear correlations, $\xi > 1$. Before we evaluate an appropriate choice for R_p we must choose a correlation function estimator.

3.3. Galaxy-Galaxy Clustering

The optimal choice of a statistical estimator of the correlation function depends on the application. With point data the basic procedure is to determine the average number of neighboring galaxies within some projected radius, r_p , and redshift distance R_p . The ij pair is weighted as $w_i w_j$ and the sum over all sample pairs is DD (Peebles 1980). A random sample of redshifts following the fitted $n(z)$ is generated along with xy co-ordinates in the visible sky area of the catalogue. We then compute the average number of random sample galaxies within precisely the same volume, assigning the random points unit weight. This average is known as DR. Then, we estimate $w_p(r_p)$ using the simplest and computationally inexpensive estimator,

$$w_p = \frac{DD}{DR} - 1, \quad (6)$$

which is accurate for the nonlinear clustering examined here and faster than methods which include the RR, *i.e.* random-random pairs.. We have verified that the $DD/RR - 1$ and $(DD - 2DR + RR)/RR$ estimators give virtually identical results over the range of pairwise separations that we use in the fits, $0.16 \leq r_p \leq 5.0h^{-1} \text{ Mpc}$. These alternate estimators are known to be superior when $\xi \leq 1$, which only occurs at the outer separation limit of our measurements. We use 100,000 random objects per patch, distributed over the redshift range 0.10 to 0.65 using the fitted $n(z)$.

The DD and DR sums extend over all four patches, so that patch to patch variations in the mean volume density become part of the correlation signal. This procedure assumes that there are no significant patch-to-patch variations in the mean photometric selection function, which is supported by the absence of any significant differences in the number-magnitude relation from patch to patch. We use geometric weights alone for the results presented here. Magnitude weights give statistically identical results for the same sample of galaxies, but, as might be anticipated, the errors in the resulting determination

of the correlation evolution are nearly a factor of two larger.

Estimated projected correlation functions, in co-moving co-ordinates using $R_p = 10h^{-1}$ Mpc, are displayed for the LCRS galaxies bounded by redshifts $[0.033, 0.15]$ and seven somewhat arbitrary redshift bins for the CNOC2 data, $[0.10, 0.20, 0.26, 0.35, 0.40, 0.45, 0.55, 0.65]$ in Figure 3. These boundaries make the end bins bigger than the middle ones to reduce the variation in numbers between the bins. For the open model we found the summed geometric weights in the bins to be $[151.8, 264.4, 267.3, 471.6, 301.2, 496.7, 286.2]$, and $[172.2, 305.0, 321.1, 595.6, 368.3, 600.3, 315.4]$ for the Λ cosmology, showing the sample differences due to cosmology are quite small. Extensive testing found that provided the bins are not made significantly narrower than the adopted limits, the bin sizes make no significant difference to the results. Adjusting the bins to have nearly constant numbers makes no difference to our result. Of course the LCRS data is very important for providing a solid measurement at low redshift.

The measured w_p are fit to the projection of the power law correlation function, $\xi(r) = (\hat{r}_0/r)^{\hat{\gamma}}$, estimating both \hat{r} and $\hat{\gamma}$. The errors at each r_p are taken as $1/\sqrt{DD}$. The fits are restricted to the $0.16 \leq r_p \leq 5.0h^{-1}$ Mpc range where there are minimal complications from geometric selection effects and the correlation signal is strong. Figure 3 displays these fits as solid lines. Also shown in Figure 3 as dashed lines are fits where we have converted to standardized $\gamma = 1.8$ correlation lengths, r_0 , using $r_0 = \hat{r}_0^{\hat{\gamma}/1.8}$. All results here are derived using co-moving co-ordinates, and normalized to a Hubble constant $H_0 = 100h \text{ km s}^{-1} \text{ Mpc}^{-1}$. The results displayed in Figure 3 are derived assuming a background cosmology of $\Omega_M = 0.2, \Omega_\Lambda = 0$.

3.4. Random Errors of the Correlations

The problem of error estimates for correlation measurements remains a topic of active research. The shot noise estimate of the fractional error as $1/\sqrt{DD}$ is appropriate for weak clustering, but a substantial underestimate for strongly nonlinear clustering, where the clustering itself reduces the effective number of independent pairs. A formal error expression in terms of the three- and four-point correlation function is available (Peebles 1980) but cumbersome and computationally expensive. Resampling techniques, such as the Bootstrap and Jackknife (Efron & Tibshirani 1986), produce substantial over-estimates of the error.

A straightforward approach to error estimates is to take advantage of our sample being distributed over a number of separate patches. We separately fit each of the four CNOC2 and six LCRS patches, to obtain an r_0 for each patch or slice. The estimated error in any correlation length, r_0 , is simply,

$$\sigma_{r_0}^2 = \frac{1}{n-1} \sum_{i=1}^n [r_0(i) - \langle r_0 \rangle]^2, \quad (7)$$

where the sum extends over the $n = 4$ CNOC2 patches and $n = 6$ LCRS slices at the redshift of interest. The average correlation length in Eq. 7 is computed from the individual patches and is not equal to the correlation of the four fields combined, which is generally larger than the average since it includes the patch to patch variation in mean counts as part of the signal. Because we have only four CNOC2 patches and six LCRS strips the estimated errors will themselves have substantial fluctuations. The resulting co-moving correlation lengths for a power law model are displayed for a range of R_p in Figure 4. The open circles are the results for the four individual CNOC2 patches (the individual LCRS slices are so similar that they are not displayed). The solid points give the result from the combined data, along with the estimated error. The mean of the fitted slopes is $\gamma = 1.87 \pm 0.07$. In principle our smaller values of R_p could cause the measured w_p to miss real correlation at large r_p , leading to γ values that are systematically too large. However,

for the $R_p \geq 10h^{-1} \text{ Mpc}$ our fitted γ values have no significant dependence on R_p .

3.5. Observational Estimates of ϵ

The co-moving $r_0(z_j)$, derived from fits to the measured w_p , are in turn fit to the ϵ model by minimizing,

$$\chi^2 = \sum_j \left[\frac{r_0^\gamma(z_j)(1+z_j)^{3-\gamma} - r_{00}^\gamma(1+z_j)^{-\epsilon}}{\sigma_\xi(z_j)} \right]^2, \quad (8)$$

over the j redshift bins by varying r_{00} and ϵ . The quantity $r_0^\gamma(z_j)(1+z_j)^{3-\gamma}$ is proportional to the mean clustered physical density. The $r_0(z_j)$ are the results of the fits to the correlation measurement of the four patches combined. The $\sigma_\xi(z_j)$ are the variances estimated from the standard deviations of the r_0 values σ_{r0} , re-expressed as a variance of the correlation amplitude, $\sigma_\xi(z) \simeq [(r_0(z) + \sigma_{r0}(z))^\gamma - r_0^\gamma(z)](1+z)^{3-\gamma}$. The σ_{r0} are evaluated using Equation 7. The χ^2 statistic allows us to evaluate absolute goodness of fit, as well as determine parameter confidence intervals.

3.6. Systematic Errors of the Correlations

We can assess the effect of varying R_p in the w_p integration using the results of the fits to the ϵ model, Eq. 2. Fitted r_{00} and ϵ are displayed as a function of R_p in Figures 5 and 6. The errors are the 90% confidence intervals. No 90% confidence fits were found at R_p of 20 and 100 $h^{-1} \text{ Mpc}$, which likely reflects variations in the estimated errors more than a true failure of the model. From these two figures we conclude that $R_p = 10$ or 30 $h^{-1} \text{ Mpc}$ converge to give statistically identical values of r_{00} and ϵ . Smaller R_p values fail to include the full signal and larger R_p values give huge patch to patch variations as large voids come and go. The most conservative choice for R_p is $10h^{-1} \text{ Mpc}$, the one with the largest error in

the stable range. Figure 5 weakly suggests that somewhat larger R_p would lead to a small increase in the correlation length, to $r_{00} \simeq 5.2h^{-1}$ Mpc. We will adopt the $R_p = 10h^{-1}$ Mpc fits as our standard results, noting that the inferred ϵ have essentially no dependence on R_p .

For small survey volumes the derived correlation length tends to systematically underestimate the result from a very large area. That is, clustering is known to be significant on scales of at least $100h^{-1}$ Mpc, hence surveys smaller than that in any dimension are likely to be measuring the range of clustering about either a local valley or plateau, and not seeing the full range of clustered density. The effect of increasing survey size on correlations can be seen in Figure 7, in that the combined analysis (filled circles) generally gives correlations higher than the mean of the individual patches (other symbols). Quantitatively, the straight mean of the CNOC2 r_0 is $3.2h^{-1}$ Mpc; the median is $3.4h^{-1}$ Mpc. It is more appropriate to average together the pair counts, which is equivalent to taking the average $\langle r_0^\gamma \rangle^{1/\gamma}$ leading to an average correlation length of $3.5h^{-1}$ Mpc. Performing a joint correlation analysis of all four patches together gives an r_0 of $4.0h^{-1}$ Mpc. This raises the question as to whether the correlations have converged within the current survey. The expected variation from patch to patch for the given volumes with narrow redshift bins is about 45%, which is consistent with the difference between a correlation length of 3.5 and $4.3h^{-1}$ Mpc. In the combined sample with larger bins we expect that there could be as much as about 10% of the variance missing, which would boost the correlation lengths by another 5%.

4. The Evolution of Galaxy Clustering

The correlation lengths for CNOC2 and LCRS, derived from fitting $w_p(r_p)$ as discussed in §3.3 and analyzed in precisely the same way for our standard $R_p = 10h^{-1}$ Mpc and $Q = 1$, are shown in Figure 7 and reported in Table 1. It is immediately clear that there

is relatively little correlation evolution for high-luminosity galaxies. It must be borne in mind that the sample is defined to be a similar set of galaxies with $L \gtrsim L_*$, with luminosity evolution-compensated, that approximates a sample of fixed stellar mass with redshift. Samples which admit lower luminosity galaxies, or do not correct for evolution, or are selected in bluer pass-bands where evolutionary effects are larger and less certainly corrected, will all tend to have lower correlation amplitudes.

The χ^2 contours of the $r_{00} - \epsilon$ model fits to the measured correlations of §3 are shown in Figure 8. At redshifts beyond 0.1 or so, the choice of cosmological model has a substantial effect on the correlation estimates. Relative to a high matter density cosmological model, low density and Λ models have larger distances and volumes, which cause the correlations to be enhanced. The LCRS data are analyzed only within the $\Omega_M = 0.2, \Omega_\Lambda = 0$ model. The correlations for three cosmologies, flat matter dominated, open, and low-density Λ , are shown in Figure 9. The χ^2 contours at the 68%, 90% and 99% contours are shown in Figure 8. The best fit ϵ value is -0.17 ± 0.18 for $\Omega_M = 0.2, \Omega_\Lambda = 0$ with $r_{00} = 5.03 \pm 0.08 h^{-1}$ Mpc. The evolution rates for the flat matter dominated and flat low-density models are $\epsilon = +0.8 \pm 0.22$ and $\epsilon = -0.8 \pm 0.19$, respectively, with r_{00} of $5.30 \pm 0.1 h^{-1}$ Mpc and $4.85 \pm 0.1 h^{-1}$ Mpc, respectively. These are marked with plus signs in Figure 8.

The effects of alternate values for the luminosity evolution are shown in Figure 8 with crosses indicating the results for $Q = 0$ and $Q = 2$, with the adopted value being $Q = 1$. The absolute magnitude limit remains $M_R = -20$ mag in all cases and we use the $\Omega_M = 0.2, \Omega_\Lambda = 0$ cosmology. For $Q = 0$ the summed bin weights are [176.1, 329.2, 347.7, 659.7, 417.7, 673.6, 318.4] and for $Q = 2$ they are [128.7, 203.7, 190.2, 317.6, 191.2, 296.0, 159.3]. The effect is that less (more) evolution compensation gives rise to a more (less) rapid decline in the correlations with increasing redshift. In

the absence of any allowance for luminosity evolution, $Q = 0$, galaxies of lower luminosity are included with increasing numbers at higher redshift. Galaxy correlations tend to decline slightly with decreasing luminosity with the strongest declines being at high-luminosity (Loveday et al. 1995) although the details of this important effect remain controversial. A preliminary investigation finds a small effect in the CNOC2 sample (Carlberg et al. 1998). If we do not correct for luminosity evolution, then intrinsically lower luminosity galaxies are included in increasing numbers at higher redshifts, which will lead to an increased rate of decline of correlations with redshift, as we have empirically demonstrated here. The observed effect over the 0.0 to 0.65 redshift range is approximately $\Delta\epsilon \approx -0.3\Delta Q$. This effect is partially responsible for the difference between the results here and those of LeFèvre *et al.* (1996).

5. Comparison of Observations and Theory

We now can compare our measurements of clustering evolution to the various simple theoretical models and analytic fits to n-body simulation results. We will cast these predictions into the form of an equivalent theoretical ϵ_T using,

$$\xi(r, z_2) = \xi(r, z_1) \left(\frac{1 + z_2}{1 + z_1} \right)^{-(3+\epsilon_T-\gamma)}, \quad (9)$$

where we have assumed that the correlation function will always be of the form $r^{-\gamma}$. Linear growth is the simplest case,

$$\xi(r, z) = D^2(z, \Omega) \left(\frac{r_{00}}{r} \right)^\gamma, \quad (10)$$

where $D(z, \Omega)$ is the linear perturbation growth factor (Peebles 1980; Peebles 1993). For the $\Omega_M = 1$, $\Omega_\Lambda = 0$, $D(z)$ is simply the expansion factor, $a(z) = (1 + z)^{-1}$, which gives the result that $\epsilon_T = 0.8$. For other Ω values we approximate the redshift dependence as a power law in $1 + z$ by evaluating the growth factor at $z = 0$ and $z = 0.5$, as is appropriate for this survey. The results are presented in Table 2.

An alternate clustering model is to allow for some bias, $b(z)$, of galaxies clustering with respect to the dark matter, $\xi_{gg} = b^2 \xi_{\rho\rho}$. There are two simple forms which describe the bias, $b(z)$, (Mo & White 1996),

$$b_{MW}(z) = 1 - \frac{1}{\delta_c} + \frac{\delta_c}{D^2(z)\sigma^2(M)}, \quad (11)$$

where $\sigma(M)$ is the tophat mass variance (Bardeen et al. 1986) in a sphere of radius $R = 1/\Omega_M^{1/3} h^{-1}$ Mpc and the critical linear overdensity, $\delta_c \simeq 1.68$. A refinement to this formula based on fitting to n-body results is (Jing 1998),

$$b_J(z) = b_{MW}(z) \left(1 + \frac{0.5 D^4(z) \sigma^4(M)}{\delta_c^4} \right)^{0.06 - 0.02n}, \quad (12)$$

where $n = d \ln \sigma^2(R) / d \ln R - 3$ is the effective index of the perturbation spectrum. We use the fit to CDM spectrum of Efstathiou, Bond & White (1992) to evaluate our tophat variances.

One possibility of relevance only in an $\Omega_M = 1$ cosmology, is that clustering obeys a scaling law (Peebles 1980; Efstathiou Davis White & Frenk 1985), $\xi(r, t) = \xi(s)$, with

$$s \propto r(1+z)^{2/(n+3)}. \quad (13)$$

CDM has such a large negative effective index, $n \simeq -2.1$ on galaxy scales, that it gives rise to a very large theoretical value of $\epsilon_T \simeq 7$, as was seen in the early CDM simulations (*e.g.*, Davis et al. 1985). An ϵ_T this large is completely excluded by clustering evolution studies.

The observations and theoretical predictions in Table 2 allow us to draw a number of conclusions. Linear theory is not a very good model because of both biasing and nonlinearities, given that the range of scales fit in the power law spans overdensities ranging from 10^3 to 0.2, but it is a useful reference point. The open and $\Omega_M = 1$ cosmologies are consistent with linear theory growth but the low density Λ model is

marginally excluded at 3.4 standard deviations (s.d.). A comparison to n-body experiments (Colin Carlberg & Couchman 1997; Colin et al. 1999; Kravtsov & Klypin 1999) shows the same approximate consistency with low density mass-traces-light cosmologies. Mo & White biasing in an open cosmology is marginally excluded at 3.8 s.d. and Jing biasing more conclusively at 4.7 s.d. Biased clustering in an $\Omega_M = 1$ cosmology is excluded at more than 6 s.d. The low density flat model is acceptable under all biasing models. Bearing in mind that the evolution of correlations is a test of both a galaxy formation and evolution model and the cosmology, these results mainly exclude models where galaxies are closely identified via the biasing mechanism with dark matter halos in an $\Omega_M = 0.2, \Omega_\Lambda = 0$, cosmology or in an $\Omega_M = 1$ cosmology. The problem in both cases is that they predict almost no correlation evolution, whereas we observed a small but significant decrease of the co-moving correlation length with redshift.

6. Conclusions

The CNOC2 redshift survey has measured precision velocities for more than 6000 galaxies in the redshift 0.1 to 0.7 range. The sky area of about 1.55 square degrees therefore covers a volume of about $0.5 \times 10^6 h^{-3} \text{Mpc}^3$. We have defined a volume limited subsample of those galaxies with k-corrected and evolution corrected R-band absolute magnitudes of $M_R^{k,e} \leq -20$ mag, where $M_* \simeq -20.3$ mag in the R-band. This subset contains about 2300 galaxies in the 0.1 to 0.65 redshift range. At low redshift we add about 13000 identically selected galaxies from the LCRS.

The correlation measurements from this paper are contained in Figure 7 and the associated Table 1. Over the redshift range examined, the correlation evolution can be described with the double power law model, $\xi(r|z) = (r_{00}/r)^\gamma (1+z)^{-(3+\epsilon-\gamma)}$, in co-moving co-ordinates. We measure a $\gamma = 1.87 \pm 0.07$ and set $\gamma = 1.8$ for fitting purposes. Our results

for various cosmologies and evolution corrections are shown in Figure 8. The primary conclusion is that correlations show a weak decline with redshift. Furthermore, there is no evidence in the current data for a change in the slope of the correlation function with redshift.

These observations test both the amplitude and redshift evolution of clustering predictions. They jointly constrain the cosmology and the galaxy formation history, and do not provide any strong constraints on the background cosmology by themselves. The comparison of our measurements and analytic fits is presented in Table 2. The correlation amplitude and slope are in quite good agreement with appropriately selected dark matter halos in a CDM simulation (Pearce et al. 1999), however the agreement depends fairly sensitively on the mass range selected (Kauffmann et al. 1999). The rate decline of clustering with redshift is slow but significant in all cosmologies examined here. That is, ϵ is always greater than -1.2 , the value for a fixed co-moving clustering length. The prediction of a slower clustering evolution in a biased $\Omega_M = 1$ cosmology is completely excluded by the more rapid decline measured here and somewhat marginally excluded in an $\Omega_M = 0.2, \Omega_\Lambda = 0$ cosmology. The models of biased clustering is an $\Omega_M = 0.2, \Omega_\Lambda = 0.8$ cosmology are statistically consistent with our measurements.

This research was supported by NSERC and NRC of Canada. HL acknowledges support provided by NASA through Hubble Fellowship grant #HF-01110.01-98A awarded by the Space Telescope Science Institute, which is operated by the Association of Universities for Research in Astronomy, Inc., for NASA under contract NAS 5-26555. We thank the CFHT Corporation for support, and the operators for their efficient control of the telescope.

REFERENCES

- Bardeen, J. M., Bond, J. R., Kaiser, N. & Szalay, A. S. 1986, ApJ, 304, 15
- Baugh, C. M., Benson, A. J., Cole, S., Frenk, C. S., & Lacey, C. G. 1999, MNRAS, 305, L21
- Broadhurst, T. J., Ellis, R. S., & Shanks, T. 1988, MNRAS, 235, 827
- Carlberg, R. G. & Couchman, H. M. P. 1989, ApJ, 340, 47
- Carlberg, R. G. 1991, ApJ, 367, 385
- Carlberg, R. G., Cowie, L., L., Songaila, A., & Hu, E. M. 1997, ApJ, 483, 538
- Carlberg, R. G., Yee, H. K. C., Morris, S. L., Lin, H., Sawicki, M., Wirth, G., Patton, D.,
Shepherd, C. W., Ellingson, E., Schade, D., Pritchet, C. J., & Hartwick, F. D. A.
1998, Phil. Trans. Roy. Soc. Lond. A. 357, 167
- Colin, P., Carlberg, R. G., & Couchman, H. M. P. 1997, ApJ, 390, 1
- Colin, P., Klypin, A., Kravtsov, A., & Khokhlov, A. 1999, ApJ, 523, 32
- Connolly, A. J., Szalay, A. S. & Brunner, R. J. 1998, ApJ, 499, L125
- Cowie, L. L., Songaila, A., Hu, E. M., & Cohen, J. G. 1996, AJ, 112, 839
- Davis, M. & Peebles, P. J. E. 1983, ApJ, 267, 465
- Davis, M., Efstathiou, G., Frenk, C. S. & White, S. D. M. 1985, ApJ, 292, 371
- Efron, B. & Tibshirani, R. 1986, *Statistical Science*, 1, 54
- Efstathiou, G., Bond, J. R. & White, S. D. M. 1992, MNRAS, 258, 1P
- Efstathiou, G., Davis, M., White, S. D. M. & Frenk, C. S. 1985, ApJS, 57, 241

- Ellis, R. S., Colless, M., Broadhurst, T., Heyl, J. & Glazebrook, K. 1996, MNRAS, 280, 235
- Governato, F., Baugh, C. M., Frenk, C. S., Cole, S., Lacey, C. G., Quinn, T. & Stadel, J. 1998, Nature, 392, 359
- Groth, E. J. & Peebles, P. J. E. 1977, ApJ, 217, 385
- Hamilton, A. J. S., Matthews, A. , Kumar, P. & Lu, E. 1991, aApJ, 374, L1
- Infante, L. & Pritchett, C. J. 1995, ApJ, 439, 565
- Jenkins, A., et al. 1998, ApJ, 499, 20
- Kaiser, N. 1984, ApJ, 284, L9
- Jing, Y. P. 1998, ApJ, 503, L9
- Kauffmann, G. , Colberg, J. M., Diaferio, A. & White, S. D. M. 1999, MNRAS, 307, 529
- Koo, D. C. & Szalay, A. S. 1984, ApJ, 282, 390
- Kravtsov, A. V. & Klypin, A. A. 1999, ApJ, 520, 437
- LeFèvre, O, Hudon, D., Lilly, S. J. Crampton, D., Hammer, F. & Tresse, L. 1996, ApJ, 461, 534
- Lilly, S. J., Tresse, L., Hammer, F., Crampton, D., & Le Fevre, O. 1995, ApJ, 455, 108
- Lin, H., Yee, H. K. C., Carlberg, R. G., Morris, S. L., Sawicki, M., Patton, D., Wirth, G. & Shepherd, C. W. 1999, ApJ, 518, 533
- Loveday, J., Maddox, S. J., Efstathiou, G. & Peterson, B. A. 1995, ApJ, 442, 457
- Mo, H. J., Jing, Y. P. & Boerner, G. 1992, ApJ, 392, 452
- Mo, H. J. & White, S. D. M. 1996, MNRAS, 282, 347

- Patton, D. R., Pritchett, C. J., Carlberg, R. G., Marzke, R. O., Yee, H. K. C., Lin, H. Morris, S. L., Sawicki, M., Shepherd, C. W., & Wirth, G. D. 2000, ApJ, to be submitted
- Peacock, J. A. & Dodds, S. J. 1996, MNRAS, 280, L19
- Jenkins, A., et al. 1999, ApJ, 521, L99
- Peebles, P. J. E. 1980, *Large Scale Structure of the Universe* (Princeton University Press: Princeton)
- Peebles, P.J.E. 1993, *Principles of Physical Cosmology* (Princeton: Princeton University Press)
- Postman, M. , Lauer, T. R., Szapudi, I., & Oegerle, W. 1998, ApJ, 506, 33
- Schechter, S. A., Landy, S. D., Oemler, A., Tucker, D. L, Lin, H., Kirshner, R. P. & Schechter, P. L. 1996, ApJ, 470, 172
- Small, T. A., Ma, C. -P. , Sargent, W. L. W. & Hamilton, D. 1998, ApJ, 524, 31
- White, S. D. M., Davis, M. , Efstathiou, G. & Frenk, C. S. 1987, Nature, 330, 451
- Yee, H. K. C., Ellingson, E., & Carlberg, R. G. 1996, ApJS, 102, 269
- Yee, H. K. C., Morris, S. L., Lin, H., Carlberg, R. G., Hall, P. B., Sawicki, M., Patton, D. R., Wirth, G. D., Ellingson, E., & Shepherd, C. W. 2000, ApJSin press (astro-ph/0004026)

Table 1: Redshift Evolution of Correlations

	r_0 in h^{-1} Mpc for $\gamma = 1.8$				
$\langle z \rangle$	$\Omega_M = 0.2, \Omega_\Lambda = 0$			$\Omega_M = 1.0, \Omega_\Lambda = 0$	$\Omega_M = 0.2, \Omega_\Lambda = 0.8$
	$Q = 0$	$Q = 1$	$Q = 2$	$Q = 1$	$Q = 1$
0.10	4.75 ± 0.05	4.75 ± 0.05	4.75 ± 0.05	4.75 ± 0.05	4.75 ± 0.05
0.16	4.52 ± 0.68	4.85 ± 0.82	4.93 ± 1.08	4.67 ± 0.76	4.94 ± 0.85
0.24	4.01 ± 0.29	4.13 ± 0.35	4.03 ± 0.42	3.65 ± 0.34	4.49 ± 0.44
0.31	3.92 ± 0.20	4.14 ± 0.31	4.01 ± 0.77	3.72 ± 0.47	4.53 ± 0.21
0.38	3.94 ± 0.41	3.90 ± 0.37	4.35 ± 0.34	3.66 ± 0.31	4.53 ± 0.28
0.42	3.44 ± 0.43	3.80 ± 0.59	4.28 ± 0.73	3.58 ± 0.40	4.14 ± 0.64
0.49	3.71 ± 0.11	4.26 ± 0.18	5.01 ± 0.45	3.77 ± 0.28	4.54 ± 0.12
0.59	3.56 ± 0.25	3.68 ± 0.27	4.75 ± 0.49	3.13 ± 0.31	4.00 ± 0.34

Table 2: Comparison of Observed and Predicted ϵ values

ϵ source	$\Omega_M = 0.2, \Omega_\Lambda = 0$	$\Omega_M = 1.0, \Omega_\Lambda = 0$	$\Omega_M = 0.2, \Omega_\Lambda = 0.8$
observation	-0.17 ± 0.18	$+0.8 \pm 0.22$	-0.8 ± 0.19
linear	-0.35	$+0.80$	-0.15
MW biased	-0.88	-0.66	-0.83
Jing biased	-1.02	-1.00	-1.00
CDM scaling	—	$+7.23$	—

Fig. 1.— Absolute magnitudes in the R-band, k-corrected and evolution-compensated ($Q = 1$), versus redshift. A volume limited sample with $M_R^{k,e} \leq -20$ mag is used for all the analysis in this paper.

Fig. 2.— Maximum likelihood fit of $n(z) \propto z^2 \exp(-\frac{1}{2}[(z - z_p)/\sigma_z]^2)$ to the observed $n(z)$, where σ_z and z_p are the parameters that are varied. The best fit has $\sigma_z \simeq 0.18$ and $z_p \simeq 0.230$. The inset figure shows the 68, 90 and 99% confidence contours for the maximum likelihood fit of these data, without binning, to the model function.

Fig. 3.— The measured projected correlations, w_p , for $\Omega_M = 0.2, \Omega_\Lambda = 0$, as a function of redshift. The power law fits with unconstrained slopes are plotted as solid lines. The projected correlations derived assuming $\gamma = 1.8$ are shown as dashed lines. The lowest line is for the LCRS sample. The next seven are for the different redshift intervals of the CNOC2 survey. The point-to-point scatter gives an indication of the errors. These correlations are calculated with $R_p = 10h^{-1}$ Mpc (co-moving).

Fig. 4.— The resultant $r_0(z)$ for a range of R_p in the $w_p(r_p)$ integration. From left to right starting at the top the R_p are 5, 7, 20, 50, 70 and 99 h^{-1} Mpc. The individual sky patches 0223, 0920, 1447 and 2148, are shown with with plus, asterisk, circle and cross symbols, respectively, and the solid symbol is the result of combined patches analysis. The “standard” correlations for the adopted value of $R_p = 10h^{-1}$ Mpc are shown in Figure 7.

Fig. 5.— The derived r_{00} as a function of the integration length, R_p , used to define $w_p(r_p)$. The 90% confidence intervals are shown. Points without error flags have fits that are outside the 90% confidence interval. This most likely arises because the variances used to calculate χ^2 are estimated from the dispersion of the four patches, which will sometimes lead to erroneously small variances and hence large χ^2 values.

Fig. 6.— The derived ϵ as a function of the integration length, R_p , used to define $w_p(r_p)$.

The 90% confidence intervals are shown. Points without error flags have fits that are outside the 90% confidence interval.

Fig. 7.— The correlation lengths (normalized to $\gamma = 1.8$) as a function of redshift for $\Omega_M = 0.2, \Omega_\Lambda = 0$. The filled diamond is for the LCRS sample. The CNOC2 errors are estimated from the variance of the four sky patches (shown with plus, asterisk, circle and cross symbols for the 0223, 0920, 1447 and 2148 patches, respectively) and the six LCRS slices (not shown since the differences are small). The filled circles are the correlations from the four fields combined. Note that these are in general always larger than the mean of the individual fields, since they include field-to-field variance.

Fig. 8.— The χ^2 confidence levels for fits to the ϵ model for the $\Omega_M = 0.2, \Omega_\Lambda = 0$ model. The contours are for 68%, 90 and 99% confidence. The plus signs mark the results for $\Omega_M = 1, \Omega_\Lambda = 0$, where $\epsilon \simeq 0.8$ and $\Omega_M = 0.2, \Omega_\Lambda = 0.8$ where $\epsilon = -0.8$. The crosses show the outcome for no evolution correction, $\epsilon = 0.3$; and $Q = 2$, evolution, $\epsilon = -0.3$.

Fig. 9.— The cosmology dependence of the correlation lengths for $\Omega_M = 0.2, \Omega_\Lambda = 0$ (circles), $\Omega_M = 1, \Omega_\Lambda = 0$ (triangles) and $\Omega_M = 0.2, \Omega_\Lambda = 0.8$ (plus signs). The darkened points are from the LCRS with $\Omega_M = 0.2, \Omega_\Lambda = 0$.

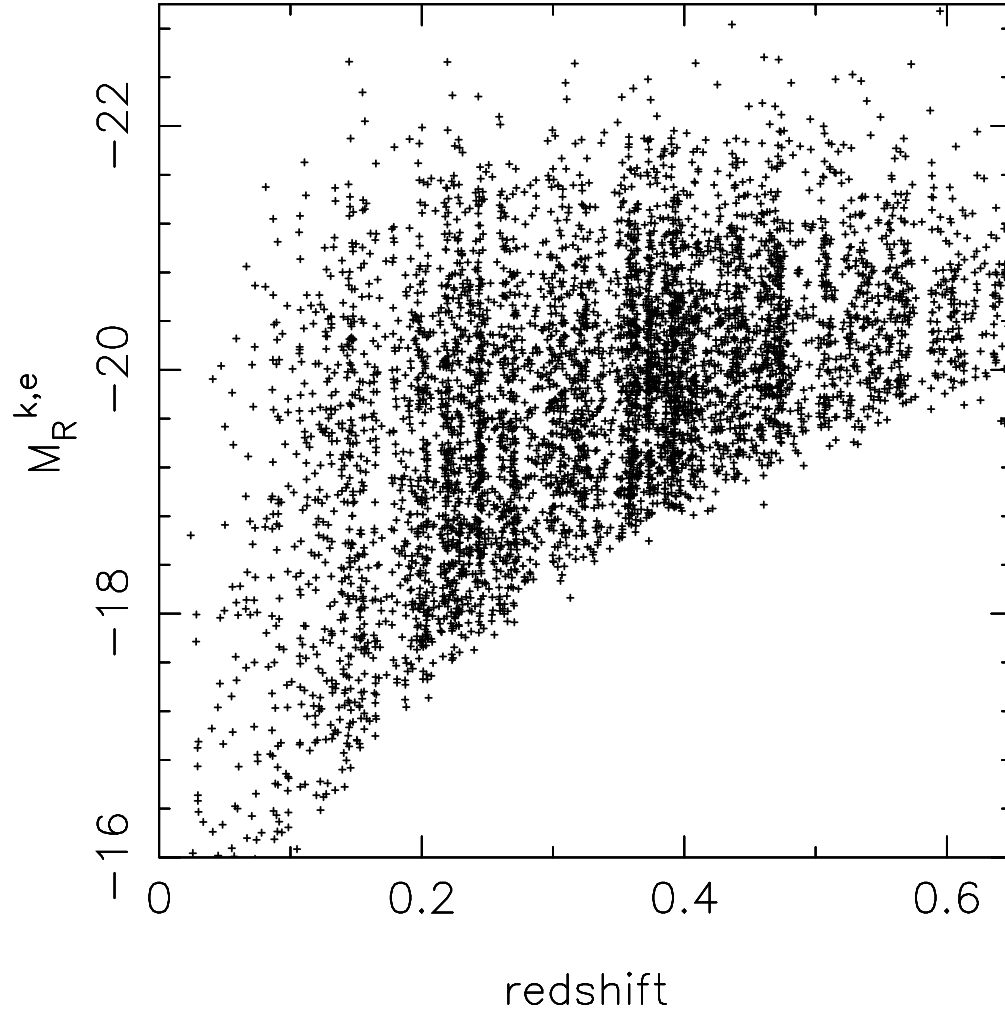


Fig. 1.—

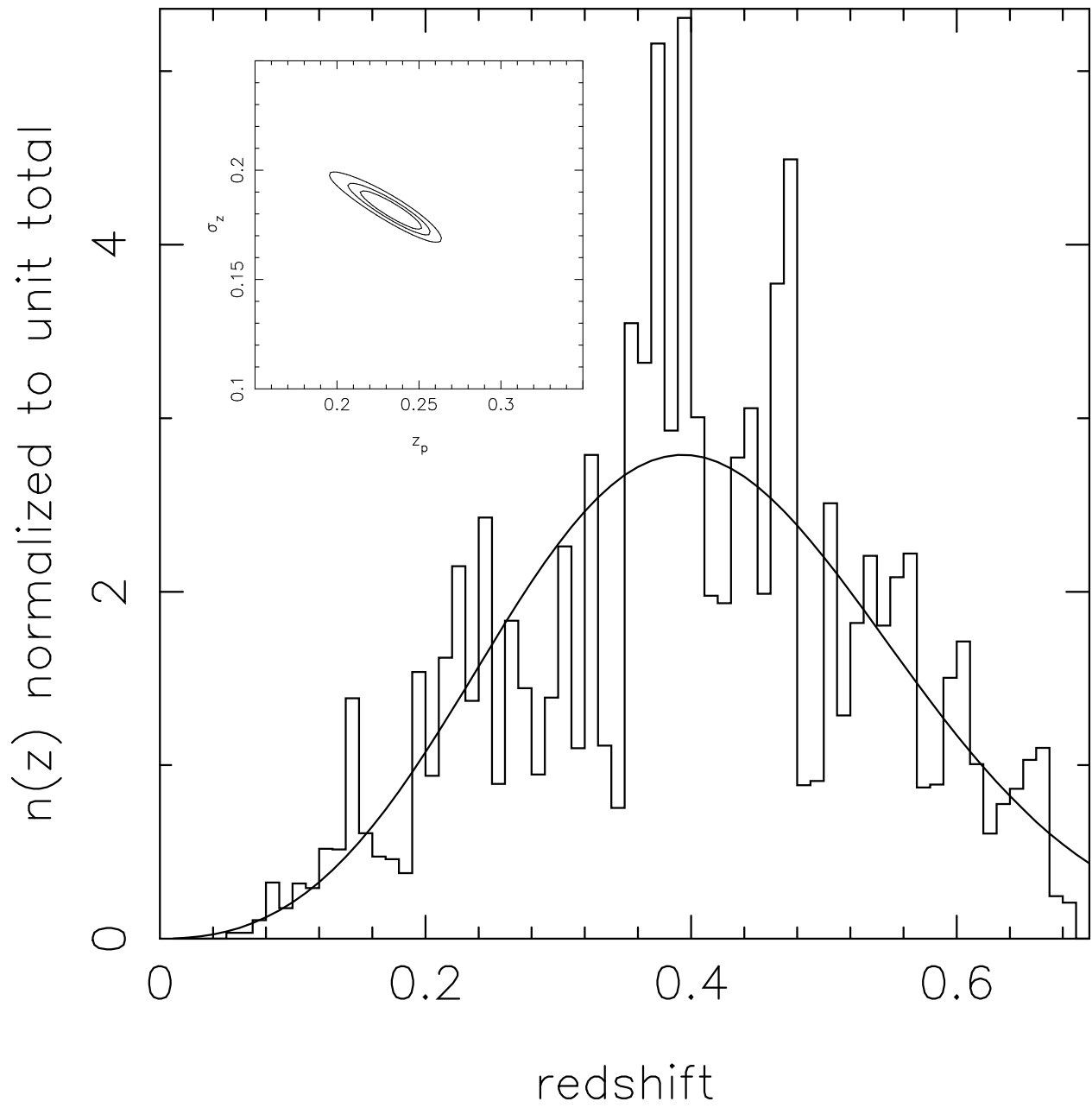


Fig. 2.—

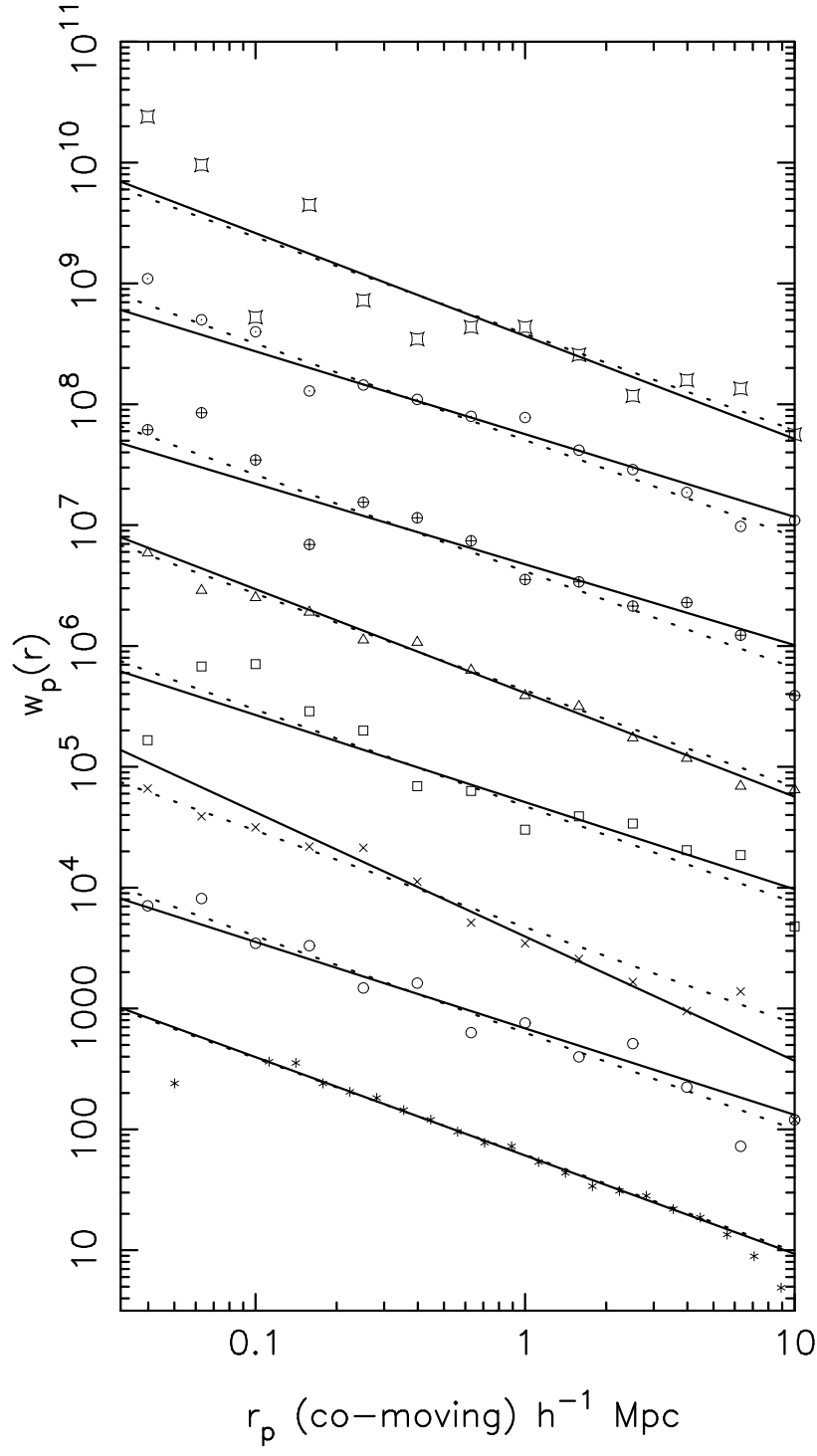


Fig. 3.—

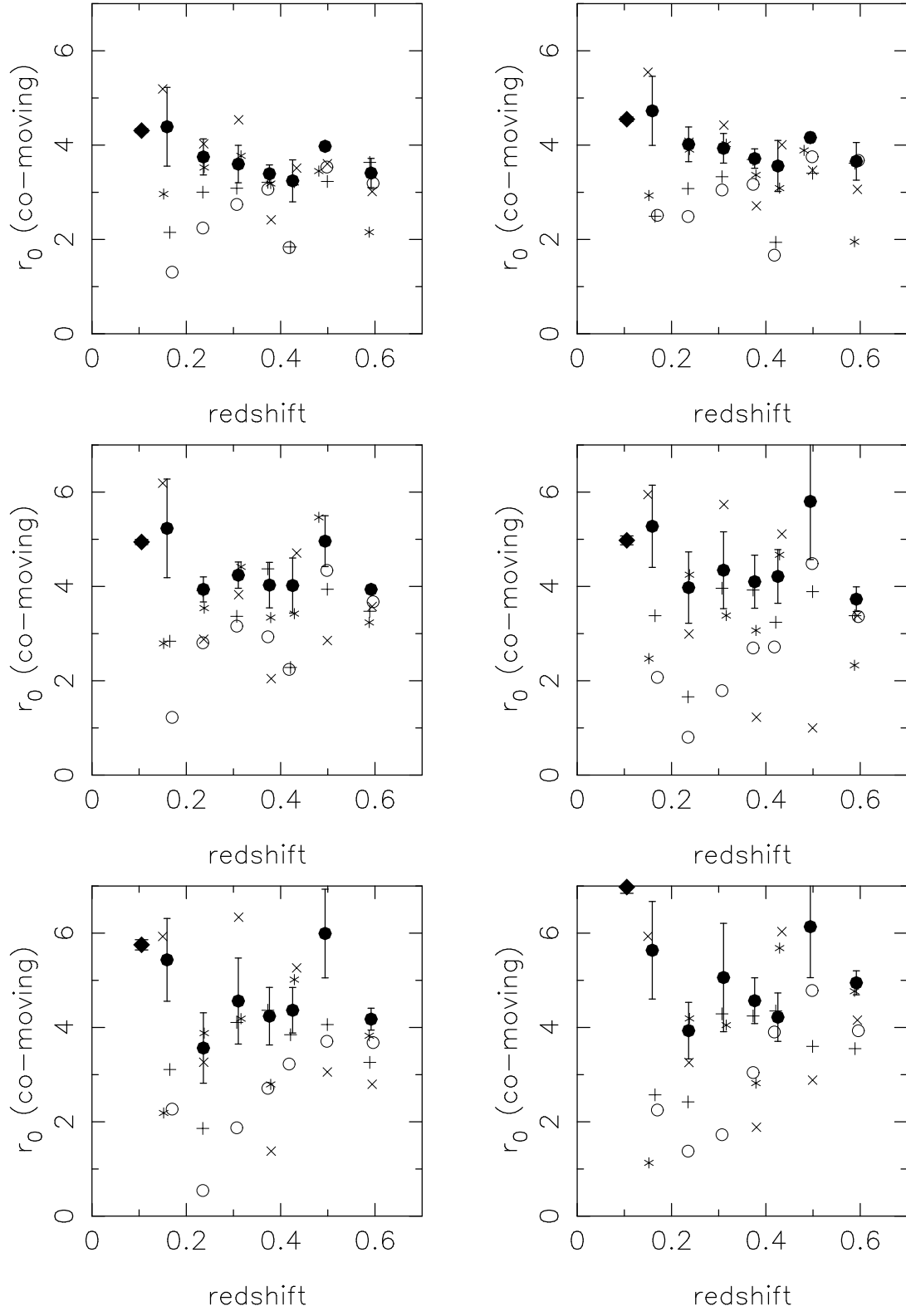


Fig. 4.—

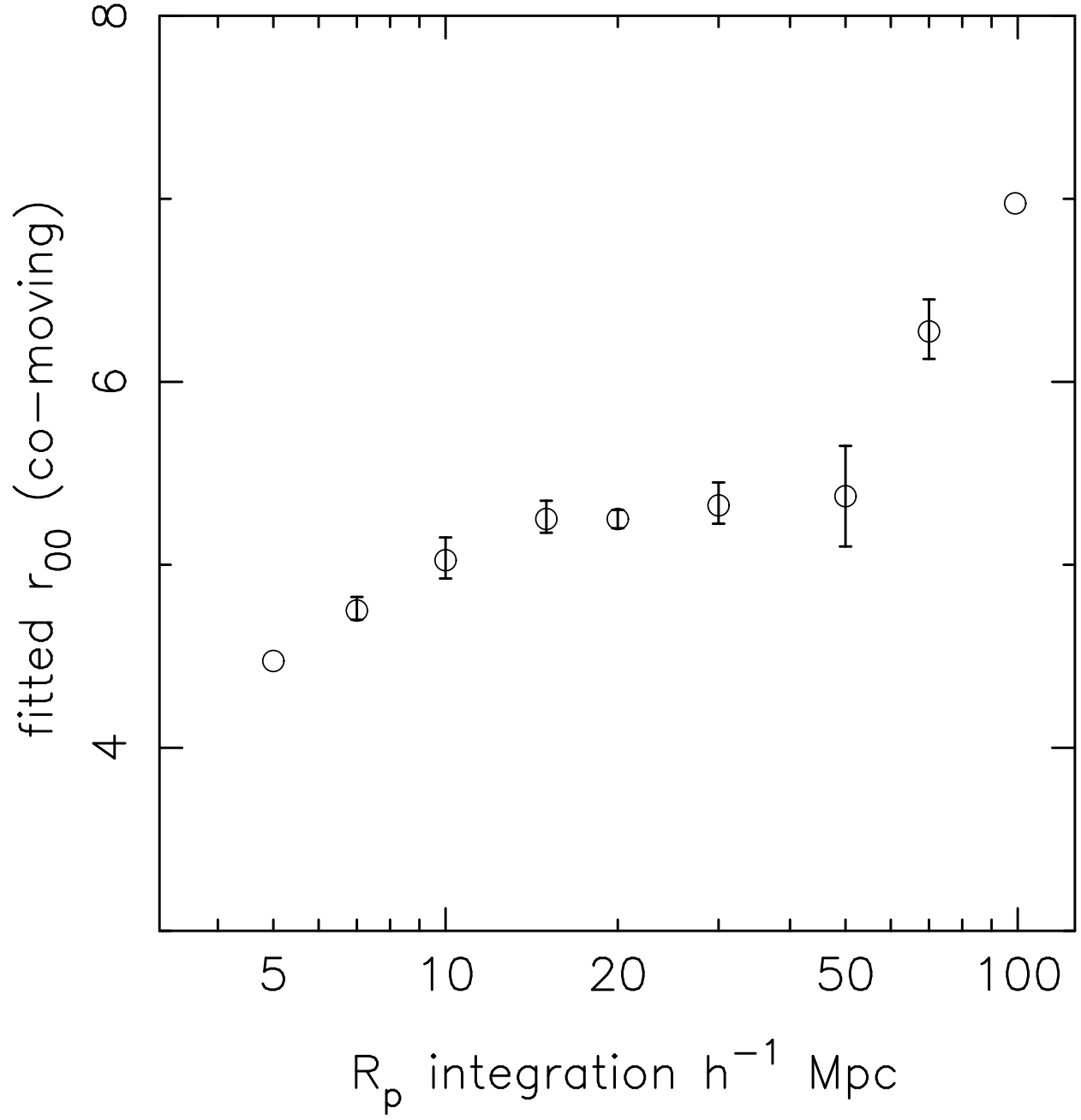


Fig. 5.—

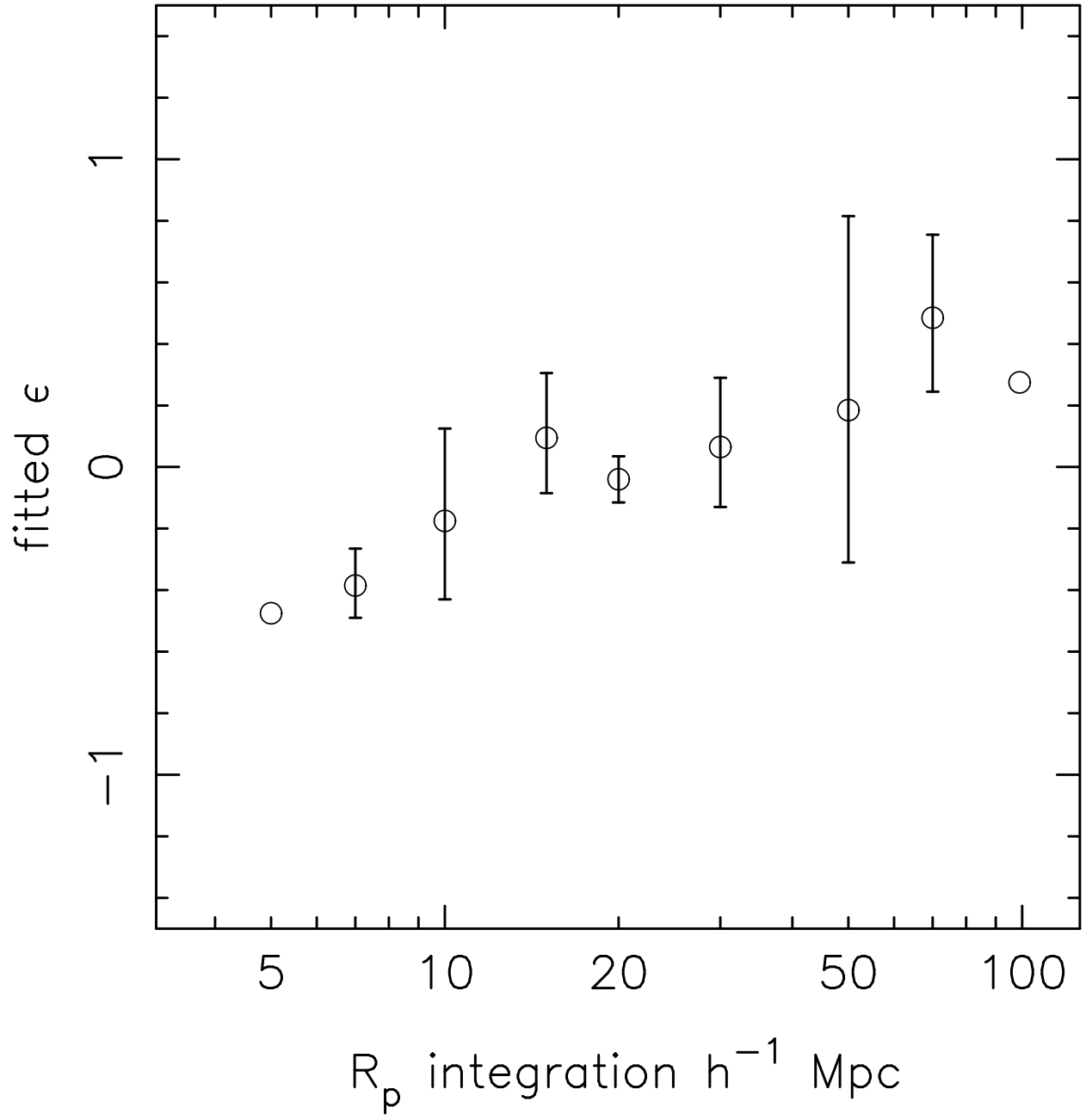


Fig. 6.—

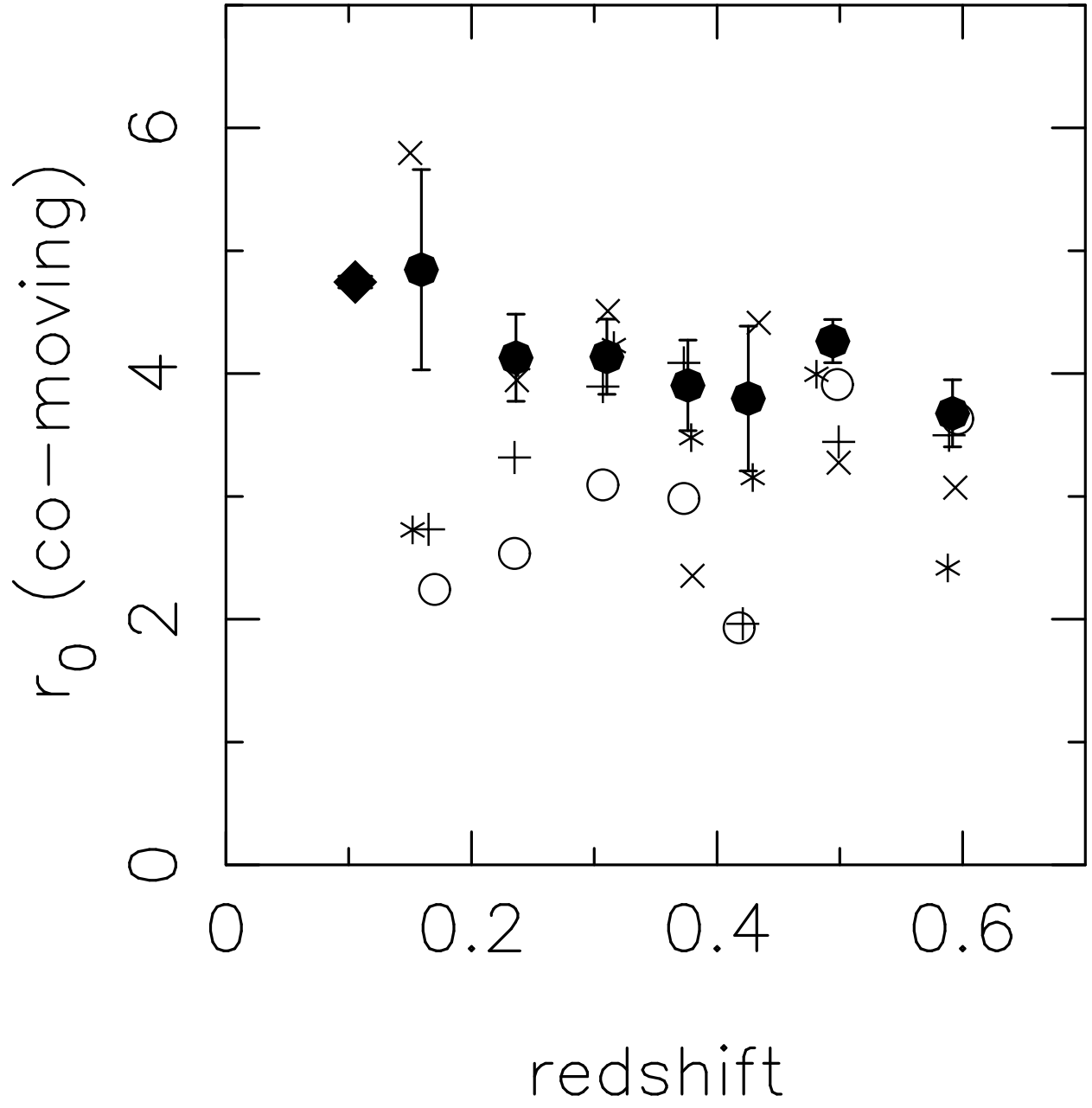


Fig. 7.—

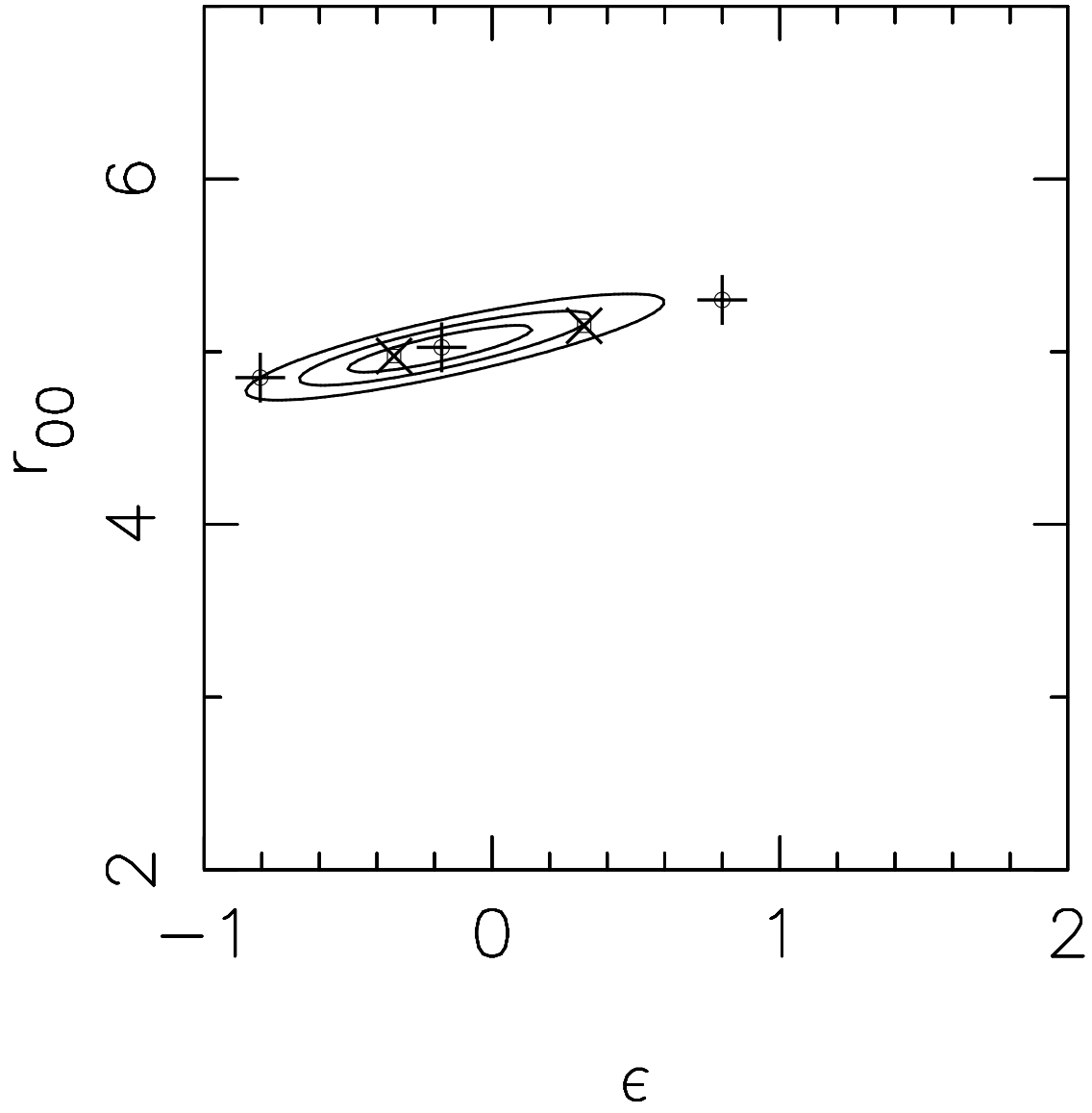


Fig. 8.—

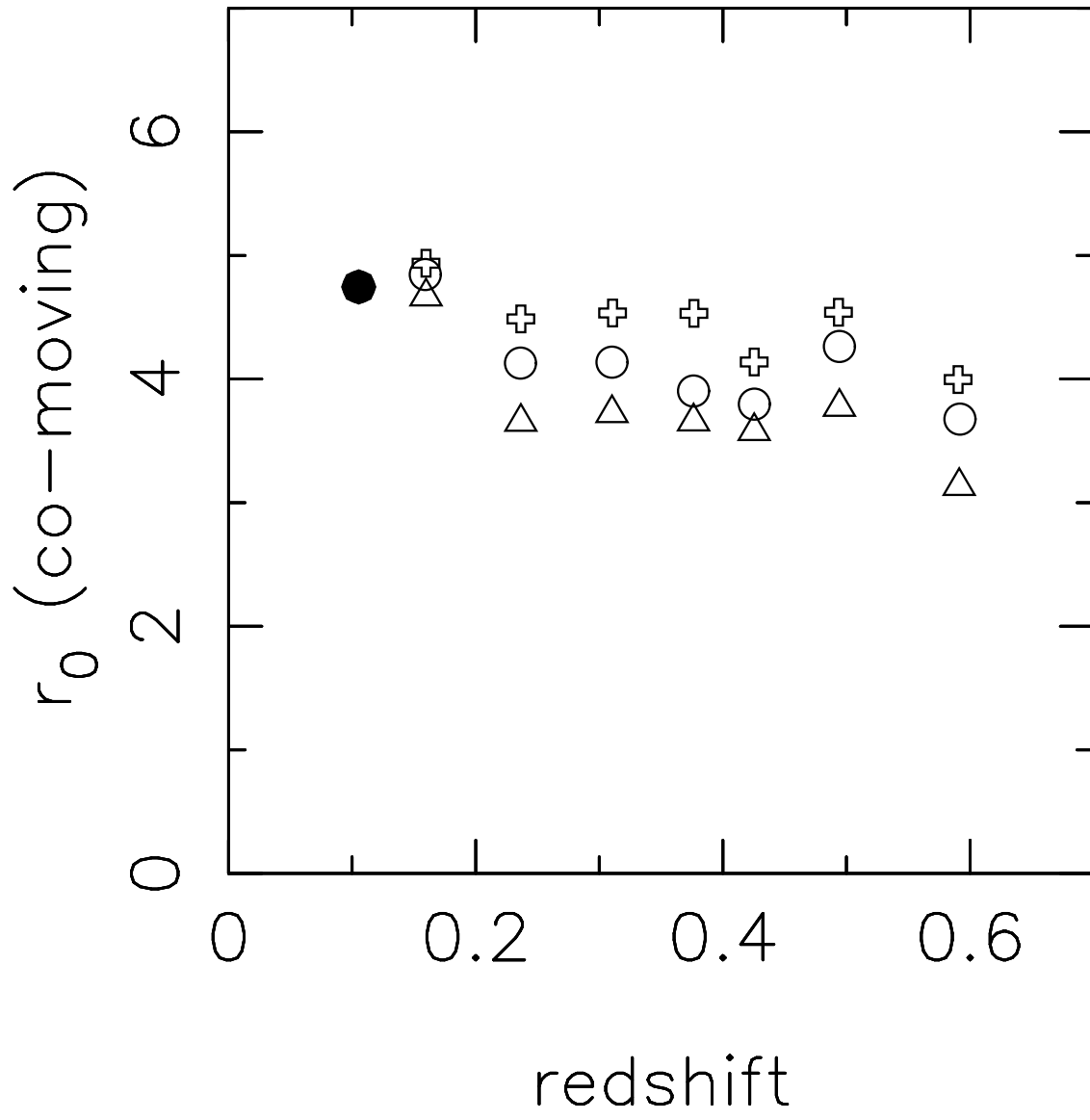


Fig. 9.—